DOUBLE–LAMBDA SENSOR PROTOTYPE FOR OPTICAL ALIGNMENT IN INHOMOGENEOUS ENVIRONMENT

Hrant Azizbekyan[1], Ara A. Grigoryan, Natella Grigoryan,
Hrant Gulkanyan, Henrik Vardanyan,
Yerevan Physics Institute after A.I. Alikhanyan,
2 Alikhanyan Brothers St., 375036 Yerevan, Armenia,
{aagrigor, nata, gulkan, henrik}@mail.yerphi.am

1. INTRODUCTION

The last decade has been marked by an intensive development of the optical systems for a high-precision monitoring of the geometry of the large-scale detectors built and being constructed for the high-energy experiments. In these systems, the light/laser beams serve as reference frames for the measurement of the detector movements at a few microns accuracy. One can mention three-point RASNIK straightness monitor of NIKHEF [1] and two-point BCAM angular monitor of the Brandeis University [2] developed for ATLAS experiment. A series of semitransparent sensors was developed by different groups for multi-point, projective monitoring of the geometry of the tracking detectors: ALMY sensor of MPI for the end-cup setup of ATLAS [3], RELMY sensor of YerPhI [4] and RELCAM monitor of Lyon-Yerevan collaboration [5] for the Tracking Chambers of the ALICE Dimuon Forward Spectrometer.

It is tacitly assumed in all these systems that the emitted light beams do not change their spatial position before being captured by sensors. This assumption can, however, be invalidated by the influence of the temperature gradients created along the light paths by the heated components of the experimental setups. These gradients can induce significant deterioration in the position of the light beams [6,7].

The effects of the medium can be distinguished from the proper movements of the monitored objects using the dispersion property of the medium [8–11]. Due to dispersion, the light beams of different wavelength deflect differently from their initial direction, giving rise to different displacements measured by the sensors and allowing to separate out the movements from the sensor data.

The dispersion method was experimentally implemented by the authors of [8–10] on the basis of dual-wavelength emitter providing a simultaneous laser radiation of two wavelengths of 860 and 430 nm. In this article, we present the tests of the feasibility of the dispersion method with a laboratory setup, which operates with infrared (IR) and ultraviolet (UV) LED sources. A short theoretical introduction to the dispersion method is presented in Section 2. The experimental setup is described in Section 3. The measurement results are exposed and discussed in Section 4. A summary and further plans are presented in Section 5.

2. THEORETICAL INTRODUCTION

Let us consider a case when the temperature gradient is directed along the y–axis. The value of the measured relative displacement Δy of two monitored objects in y–direction will then

[1] Engineering Centre of NAS of Armenia, Gitavan-2, 378410, Ashtarak, Armenia

represent superposition of the proper relative movement Δy_a and the light deflection Δy_{th}. Due to the dispersion property of the medium, the value of the measured displacement will be different for the beams with different wavelengths λ_1 and λ_2:

$$\Delta y(\lambda_1) = \Delta y_a + \Delta y_{th}(\lambda_1) \quad (1)$$

$$\Delta y(\lambda_2) = \Delta y_a + \Delta y_{th}(\lambda_2) \quad (2)$$

As it was shown in [11], the ratio of the last terms in (1) and (2), $r = \Delta y_{th}(\lambda_1)/\Delta y_{th}(\lambda_2)$, is practically independent of the temperature gradient distribution along the path of the light beams (except for the cases, when the air temperature gradient abruptly changes its direction and value in different regions of the medium traversed by the light beams) and is determined by the ratio of the thermal gradients of the air refractive index $\nabla_T n(\lambda)$:

$$r = \nabla_T n(\lambda_1)/\nabla_T n(\lambda_2) = [1 + 0.741d(\lambda_1/\lambda_{01}) + 0.023d(\lambda_1/\lambda_{02})]/[1 + 0.741d(\lambda_2/\lambda_{01}) + 0.023d(\lambda_2/\lambda_{02})] \quad (3)$$

with $d(x) = (3x^2 - 1)/(x^2 - 1)^2$, $\lambda_{01} = 0.0828$ μm and $\lambda_{02} = 0.1562$ μm. The last equality in (3) stems from the empirical parameterization of the air refractive index [12,13] (see also [11]).
Using (1) – (3), one can express the relative movement Δy_a in terms of measured displacements $\Delta y(\lambda_1)$, $\Delta y(\lambda_2)$ and ratio r:

$$\Delta y_a = (\Delta y(\lambda_1) - r\Delta y(\lambda_2))/(r - 1). \quad (4)$$

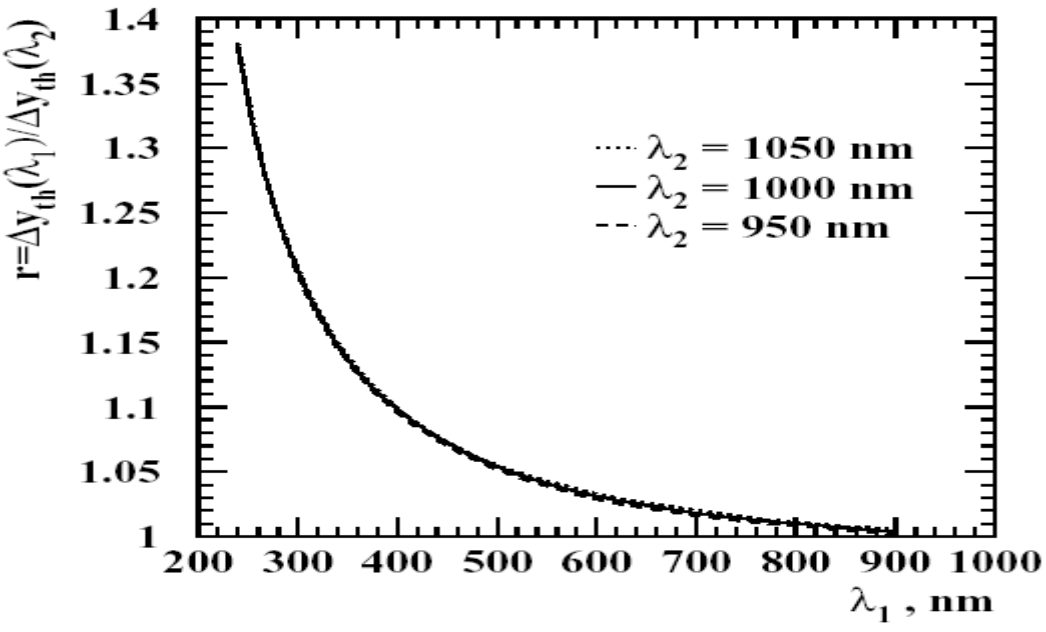

Figure 1 The ratio r, Eq. (3), as function of λ_1

The accuracy of the determination of Δy_a then reads as

$$\sigma(\Delta y_a) = \sigma_m(\sqrt{1 + r^2})/(r - 1), \quad (5)$$

where σ_m is the precision of the measurement of the values $\Delta y(\lambda_1)$ and $\Delta y(\lambda_2)$.
Figure 1 shows the dependence of r on λ_1 at different values of λ_2 taken in the IR region. It is seen that r does not practically depend on the value of the IR light wavelength, while it rapidly grows with the decrease of λ_1 in the UV region.

For the case of λ_1 = 360 nm and λ_2 = 1000 nm (exploited below), one has r = 1.128 which results in the following accuracy of the determination of Δy_a

$$\sigma(\Delta y_a) \approx 12\sigma_m \qquad (6)$$

3. EXPERIMENTAL SETUP

In order to check the feasibility of the dispersion monitoring method, an experimental laboratory setup was constructed and tested [14]. Below we present the measurements with an upgraded version of the setup. Its schematic view is shown in Figure 2. Two LED sources were used: ultraviolet, with $\lambda(UV)$ = 360 nm, and infrared, with $\lambda(IR)$ = 1000 nm. After passing through a filter (with maximal transparency for the range λ = 260 – 380 nm), the UV light is reflected from a mirror. The IR beam passes through the same mirror semitransparent in the IR region.

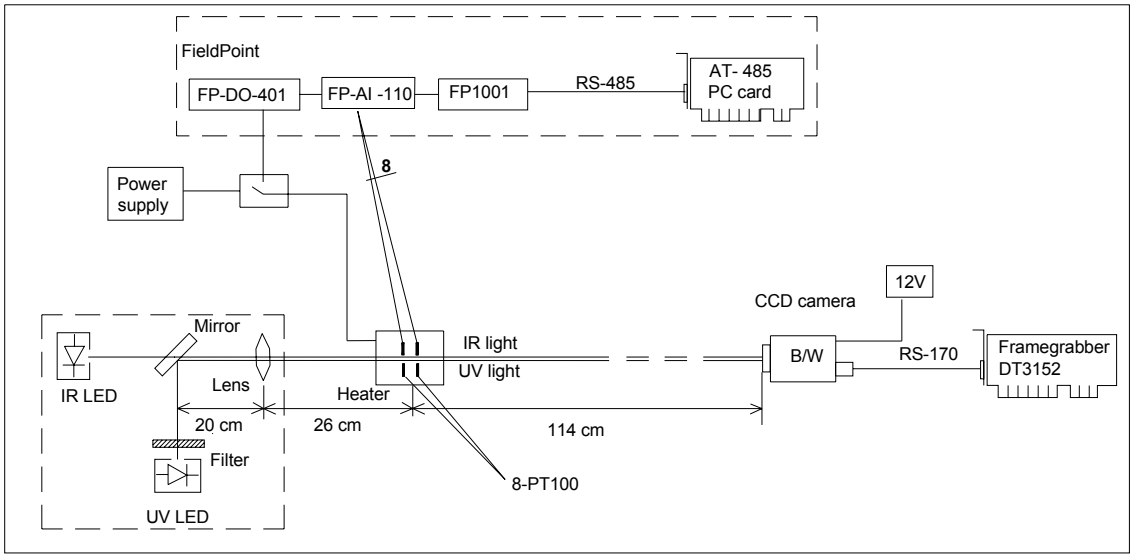

Figure 2 Schematic view of YerPhI experimental setup for dispersion measurements with IR and UV lights.

Both beams are focused by a lens (installed 20 cm downstream of the mirror) on a CCD photosensor located at z(CCD) = 1.4 m downstream of the lens. After passing the lens, both beams are directed along z–axis. They have initial diameters of about 3 mm and overlap each other along the most part of their path towards the CCD, on which their images are 2.5 mm apart. The diameters of the light spots on the CCD are about 0.5 mm.

The array size of the CCD (OS – 45D composed of 768×576 pixels with the unit cell size of 8.6×8.3 μm^2) is 6.6×4.8 mm^2 in the horizontal x– and vertical y–directions, respectively. The CCD video frame is captured by Frame Graber DT3152 (during 0.1 sec) and stored in the PC as a binary file. This file is used to determine (during 0.4 sec) the x– and y–coordinates of the light spot center of gravity.

A horizontal heating plate of 23 cm width along the light beam is installed between the focusing lens and CCD. The beams pass 13.5 mm above the heater. The distance between the heater center and the lens (CCD) is 26 (114) cm. The temperature map along the light path is measured with the help of two sets of 8 PT100 thermoresistors located at 8.5 and 18.5 mm vertical distance above the heater. The thermoresistors data are transferred to a PC by National Instruments FieldPoint modules and RS485 Network Interface. The data are analyzed by LabView program

package. The measurements of the light deflection are performed at temperature gradients $\nabla_y T$ ranging from –0.5 to –4.0^o C/cm at the point on the light trajectory situated above the geometrical center of the heater. The accuracy of $\nabla_y T$ measurement is about 10%.

4. MEASUREMENT RESULTS

The typical behaviour of the y– and x–coordinates of the light spot center of gravity on CCD is demonstrated in Figures 3 and 4, respectively. It is seen, that after switching on the heater, the y–position of the light beam shifts upward and undergoes large fluctuations (Figure 3). In what concerns the x–position (Figure 4), one does not observe regularities in the behaviour of the light spot, except fluctuations (that exceed those in the vertical direction).

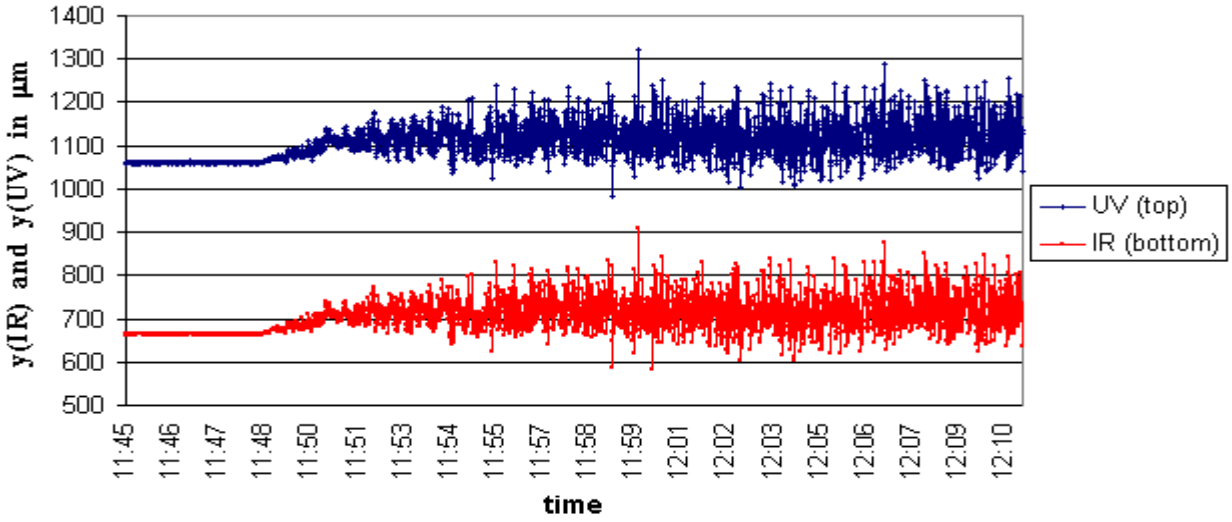

Figure 3 The y–coordinates of the IR and UV light spots before and after switching on the heater at 11:48.

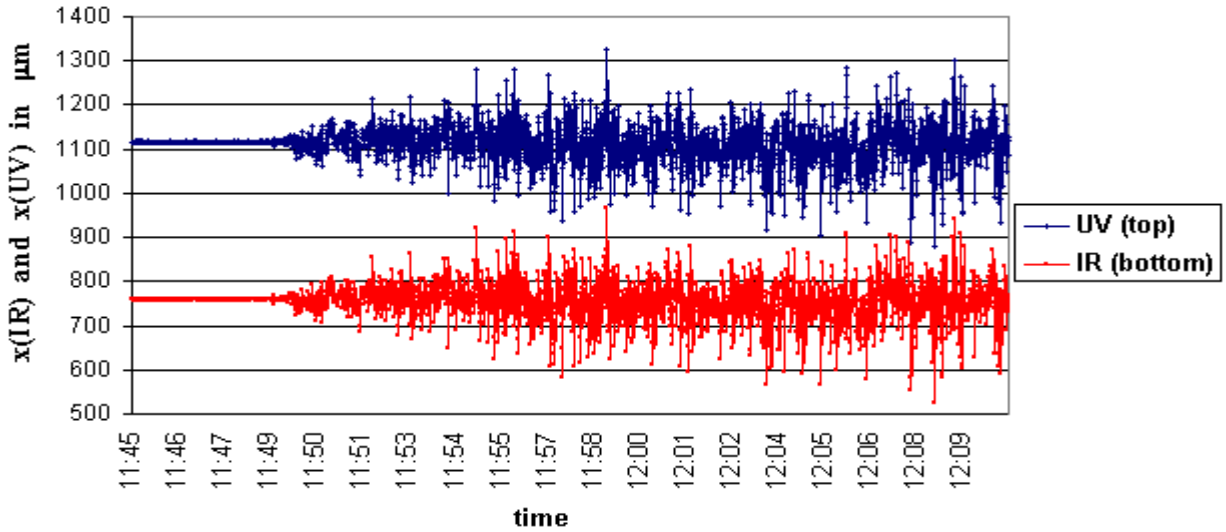

Figure 4 The x–coordinates of the IR and UV light spots before and after switching on the heater at 11:48.

Figure 5 demonstrates the temperature gradients measured in the middle of the heater. One concludes from this Figure that there are large temperature gradient fluctuations generated by the

air turbulence and that the peculiarities of the light behaviour, presented in Figures 3 and 4, can be explained by those of $\nabla_y T$ and $\nabla_x T$, respectively.
In order to reduce the effect of the temperature gradient fluctuations caused by the turbulence, the measurements of the light deflection were integrated/averaged over some time interval, using a large number n_f of the readings from CCD.

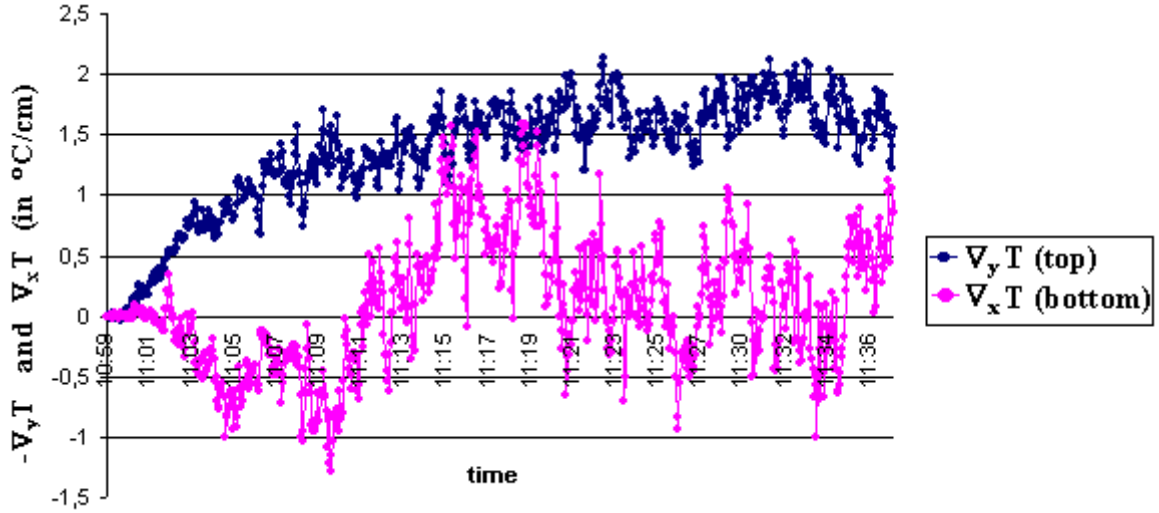

Figure 5 Time evolution of the horizontal ($\nabla_x T$) and vertical ($-\nabla_y T$) temperature gradients after switching on the heater. The time interval between two consecutive measurements is 3 sec.

The integration effect is demonstrated in Figure 6 showing the light deflections with n_f = 1 (lasting 0.1 sec) and n_f = 1000 readings (lasting about 100 sec) per point. It is seen, that the turbulence induced fluctuations are reduced by more than one order of magnitude for the integrated data which now reveal a regular upward shift of the light beam along the *y*–axis.

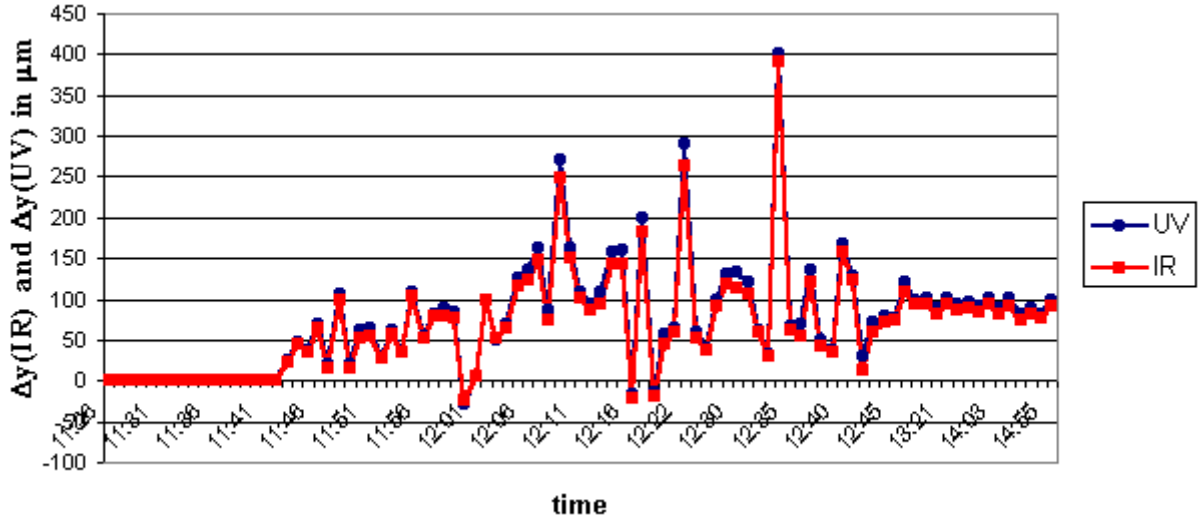

Figure 6 Deflections of the IR and UV beams measured by 1 reading (till 12:53) and 1000 readings (since 13:04). The heater is switched on at 11:42.

Two Figures below demonstrate the n_f – dependence of the precision of the light position determination in thermally homogeneous (Figure 7) and inhomogeneous (Figure 8) air environments.

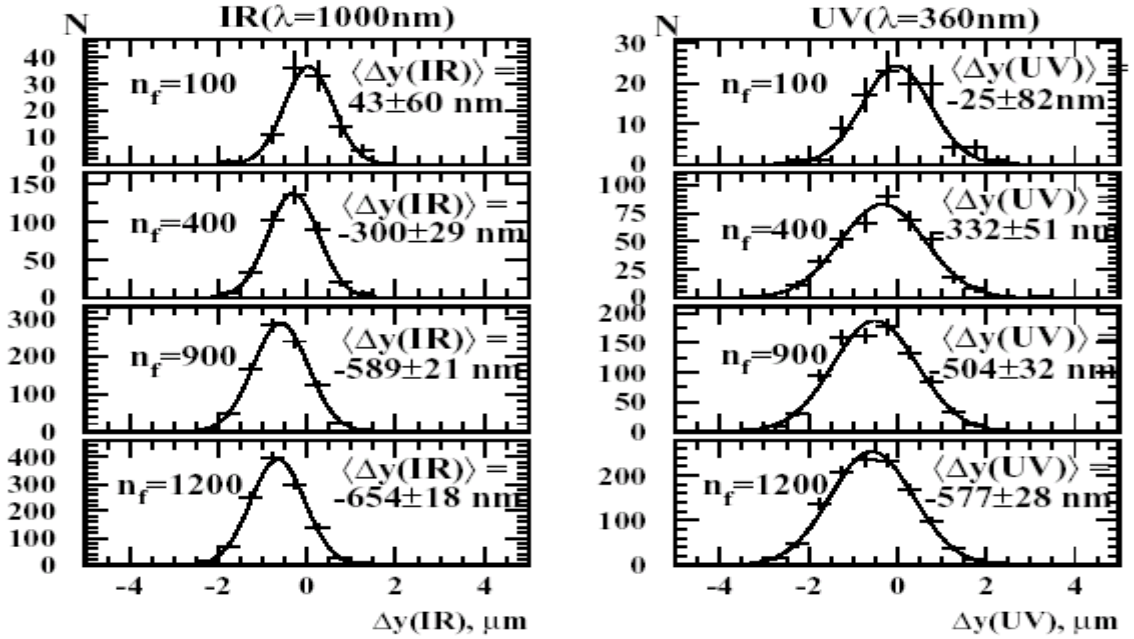

Figure 7 Accuracy of the light position measurements at heater switched off as function of the number of readings.

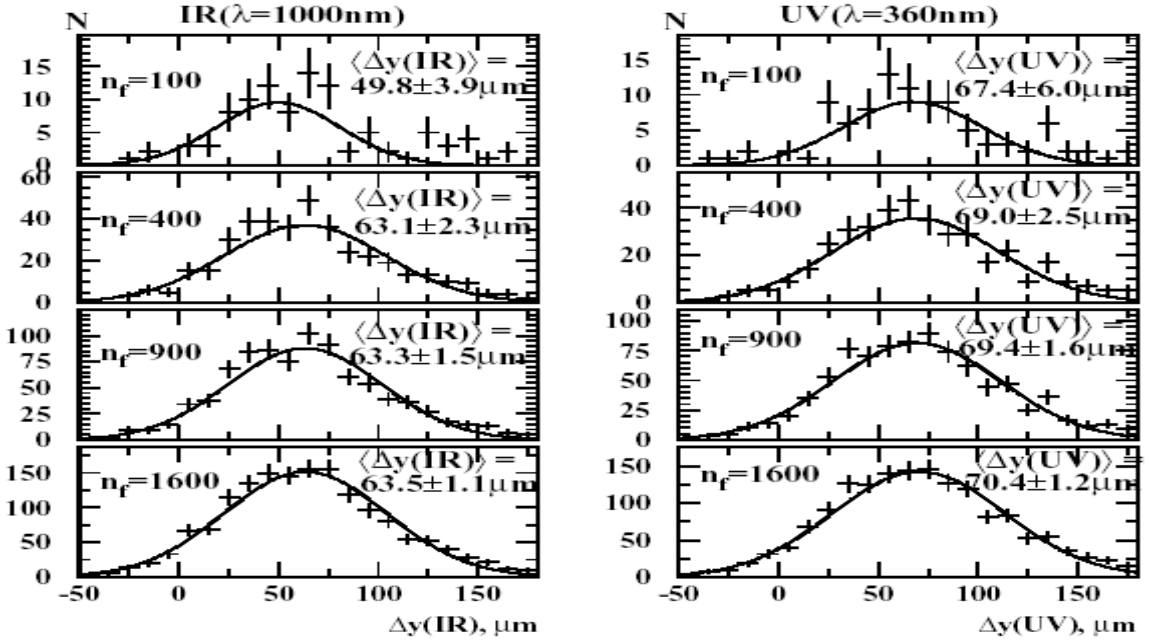

Figure 8 Accuracy of the light position measurements at heater switched on as function of the number of readings.

In the homogeneous medium (the heater is switched off), the accuracy of the determination of the mean value of the light beam position reaches 20–30 nm provided $n_f > 900$. The width of distributions shown on Figure 7 fitted by Gaussian curves is about 0.6-0.9 μm characterizing the accuracy of the measurement by a single reading from the CCD. Figure 8 demonstrates the measurement precisions in the heated medium. The single-reading accuracy worsens noticeably reaching 40 μm. However, at sufficiently large n_f (≥900), the mean value of the light beam position can be determined with a precision of about 1 μm.

Figure 9 demonstrates the temperature distribution over z (z = 0 corresponds to the geometrical center of the heater) at 4 values of the supply current measured by the thermoresistors placed at 8.5 mm (black circles) and 18.5 mm (open circles) above the heater. The z-dependence of data is approximated as a plateau in the central region of the heater plus Gaussian 'wings' outside the central region. The solid and dashed curves represent the fit of the data. The curves were used to extract the z-dependence of the gradient along the light rays which pass at y = 13.5 mm vertical distance above the heater.

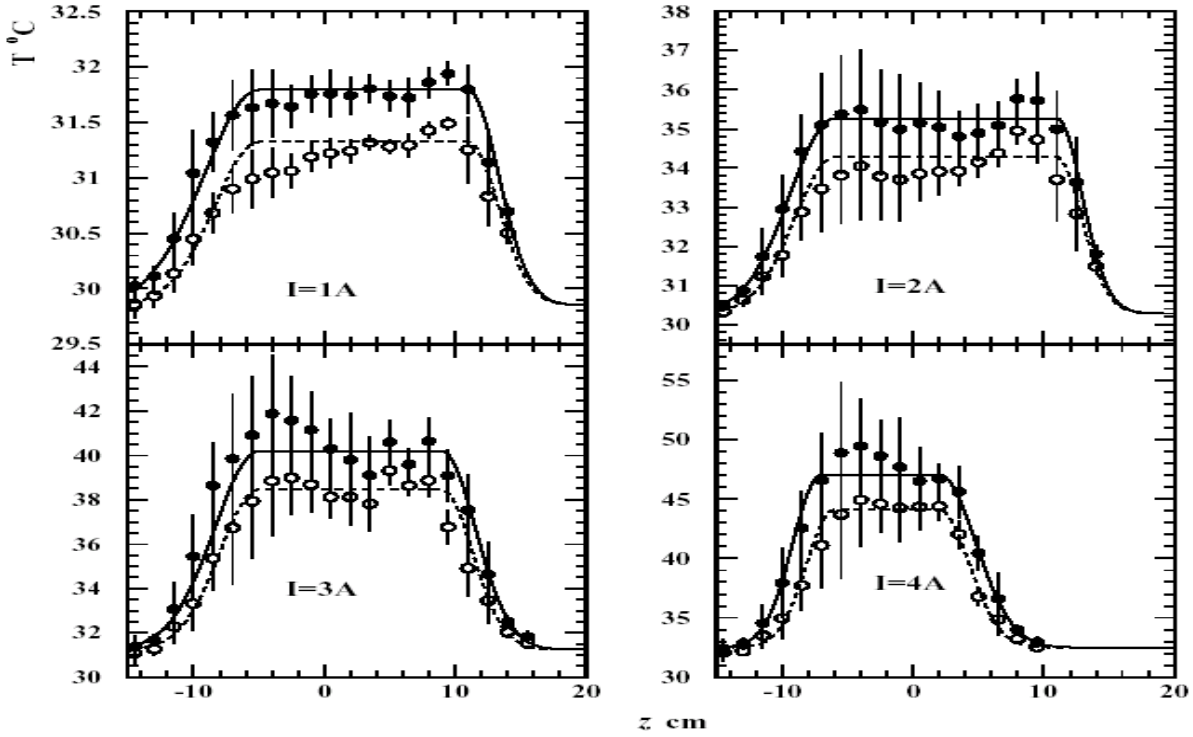

Figure 9 Distribution of the temperature over z at different supply currents (for the details see the text)

Figure 10 shows the time dependence of the light spot y–coordinates, while Figure 11 demonstrates the deflections Δy and Δx of the light beams from their initial (the heater switched off) position. The data presented in these Figures are obtained at the supply current I = 3 A by integrating over n_f = 1000 readings for each experimental point. At this supply current, the mean vertical temperature gradient, $< \nabla_y T >_0$, obtained by averaging $\nabla_y T$ over the plateau region (see Figure 9) equals -1.7^o C/cm. One sees that although the shifts $\Delta y\ (UV)$ and $\Delta y(IR)$ fluctuate over time, they are strongly correlated, with their ratio $\Delta y(UV)/\Delta y(IR)$ being, as it is expected, almost constant (see asterisks in Figure 11). When averaging over the measurement period (about 8 hours), one finds that the mean value of this ratio, $<\Delta y(UV)/\Delta y(IR)>$, is 1.128±0.006, very close to the value of $r = \Delta y_{th}(\lambda_1)/\Delta y_{th}(\lambda_2)$ = 1.128 at $\lambda(UV)$ = 360 nm and $\lambda(IR)$ = 1000 nm (see Section 2). The average values of the deflections are $<\Delta y(UV)>$ = 51.9±3.2 μm and $<\Delta y(IR)>$ = 46.0±3.0 μm, the quoted errors being the r.m.s. values characterizing the long-term variations of the temperature gradient.

The same strong correlation is seen between the deflections $\Delta x(UV)$ and $\Delta x(IR)$. However, the horizontal deflections are much smaller as compared to the vertical ones and their average values are consistent with zero (as a consequence of negligibly small average horizontal temperature gradients). The numerical values are $<\Delta x(UV)>$ = 2.5±3.7 μm and $<\Delta x(IR)>$ = –0.9±3.5 μm.

Note that the r.m.s. values for $\Delta x(UV)$ and $\Delta x(IR)$ slightly exceed those for $\Delta y(UV)$ and $\Delta y(IR)$ due to the larger fluctuations of $\nabla_x T$ (cf. Figure 5).

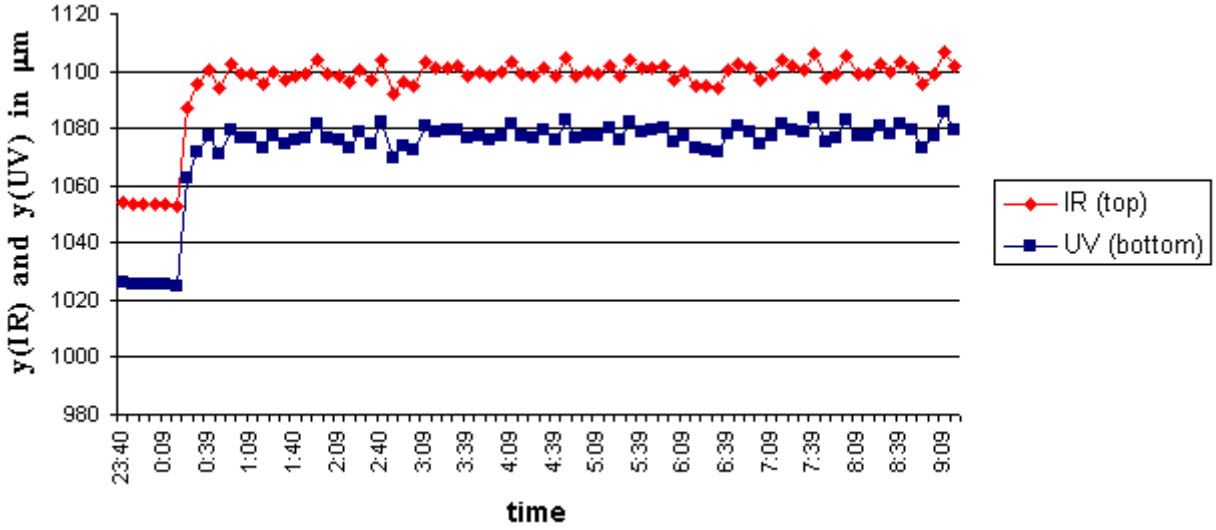

Figure 10 The *y*–position of the IR and UV lights before and after switching on the heater at 00:00 (the mean vertical temperature gradient is -1.7^{o} C/cm).

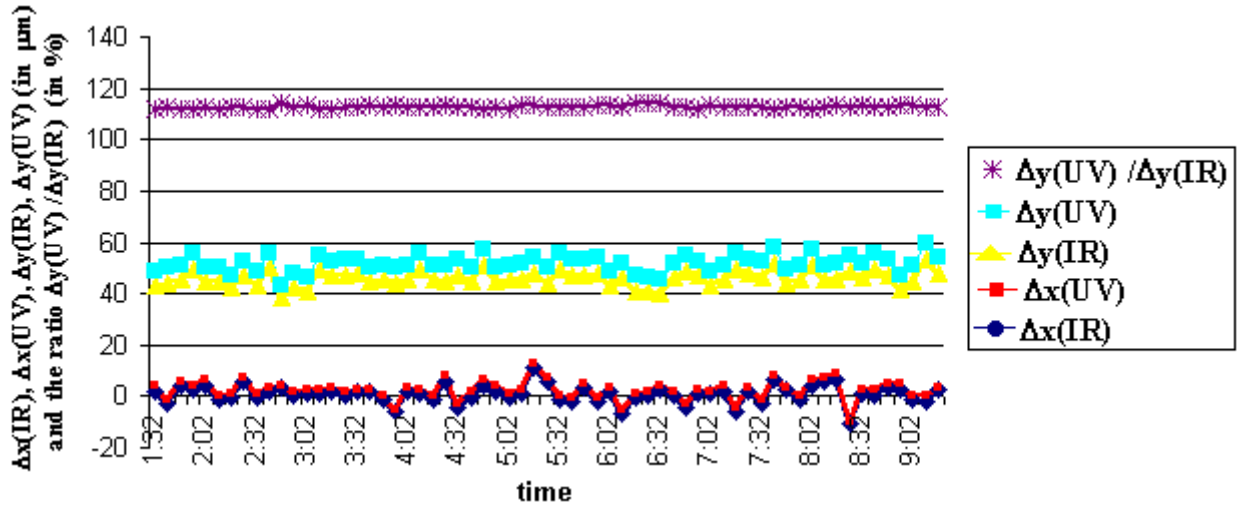

Figure 11 The IR and UV light deflections in the horizontal, *x*, and vertical, *y*, directions and the ratio $\Delta y(UV)/\Delta y(IR)$ at the mean vertical temperature gradient = – 1.7^{o} C/cm.

Analogous measurements were done at 8 more values of $<\nabla_y T>_0$ corresponding to eight different values of the heater supply current. For each of these sets, the mean values, $<\Delta y(UV)>$, $<\Delta y(IR)>$ and $<\Delta y(U)/\Delta y(IR)>$ were obtained by averaging over the whole measurement period which lasted up to 8 hours. The theoretical predictions on the dependence of $<\Delta y(UV)>$ and $<\Delta y(IR)>$ on $<\nabla_y T>_0$ are compared with the measurement results in the top part of Figure 12. The theoretical curves (solid (dashed) line for UV (IR) light) are calculated on the basis of the formulae from Appendix B of [11] taking into account the geometry of the setup and the measured temperature map at each supply current. A good agreement is seen between the predicted and measured dependence of the deflections on the value of the mean vertical temperature gradient. Deviation from straight lines is caused by the irregular shapes of the measured temperature map at different supply currents, which leads to the irregularities in the

predicted light deflections. The bottom part of the Figure 12 shows the dependence of the ratio $<\Delta y(U)/\Delta y(IR)>$ on $<\nabla_y T>_0$. It is seen that this ratio is practically independent of $<\nabla_y T>_0$, being, with some exceptions, consistent with the value of $r = \Delta y_{th}(\lambda_1)/\Delta y_{th}(\lambda_2) = 1.128$ expected for the thermal deflections of $\lambda(UV) = 360$ nm and $\lambda(IR) = 1000$ nm lights (see Section 2).

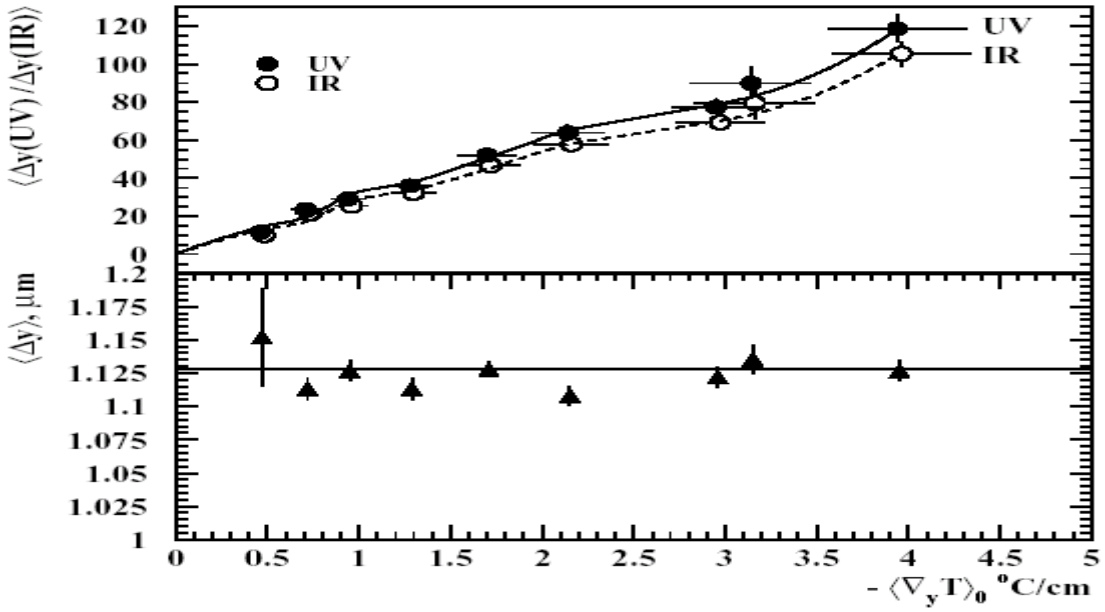

Figure 12 Dependence of the UV and IR light *y*–deflections (top) and of their ratio (bottom) on the mean vertical temperature gradient.

Another form of the comparison of the experimental and theoretical values of the light deflections is presented in Figure 13. It is seen that the data are well fitted by the diagonal, the line of the equality of measured (vertical axis) and calculated (horizontal axis) values.

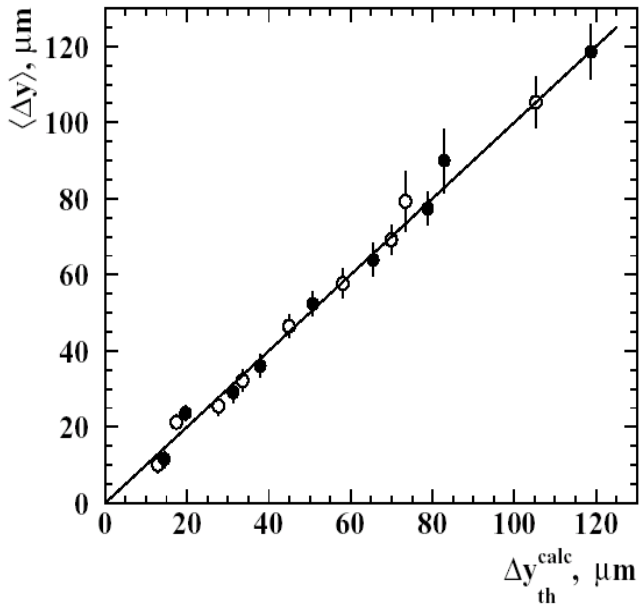

Figure 13 The measured mean deflections of the UV (black circles) and IR (open circles) light beams versus the calculated deflections at different mean temperature gradients (cf. Figure 12).

One should note that although the light sources and CCD were fixed at their places during the whole measurement period, possible relative instabilities caused by various incontrollable sources could take place. In order to estimate these instabilities, one has to infer, with the help of Eq. (4) at $r = 1.128$, the values of the relative movements of the light source and photosensor in the horizontal and vertical directions. We consider first the data presented in Figures 7 and 8. For these data, the distributions of the reconstructed relative movements in the vertical direction, Δy_a, are shown in Figure 14 at different values of n_f for both homogeneous and heated cases. The width of these distributions fitted by Gaussian curves is about 8 μm for the homogeneous case and 34 μm for the inhomogeneous air medium.

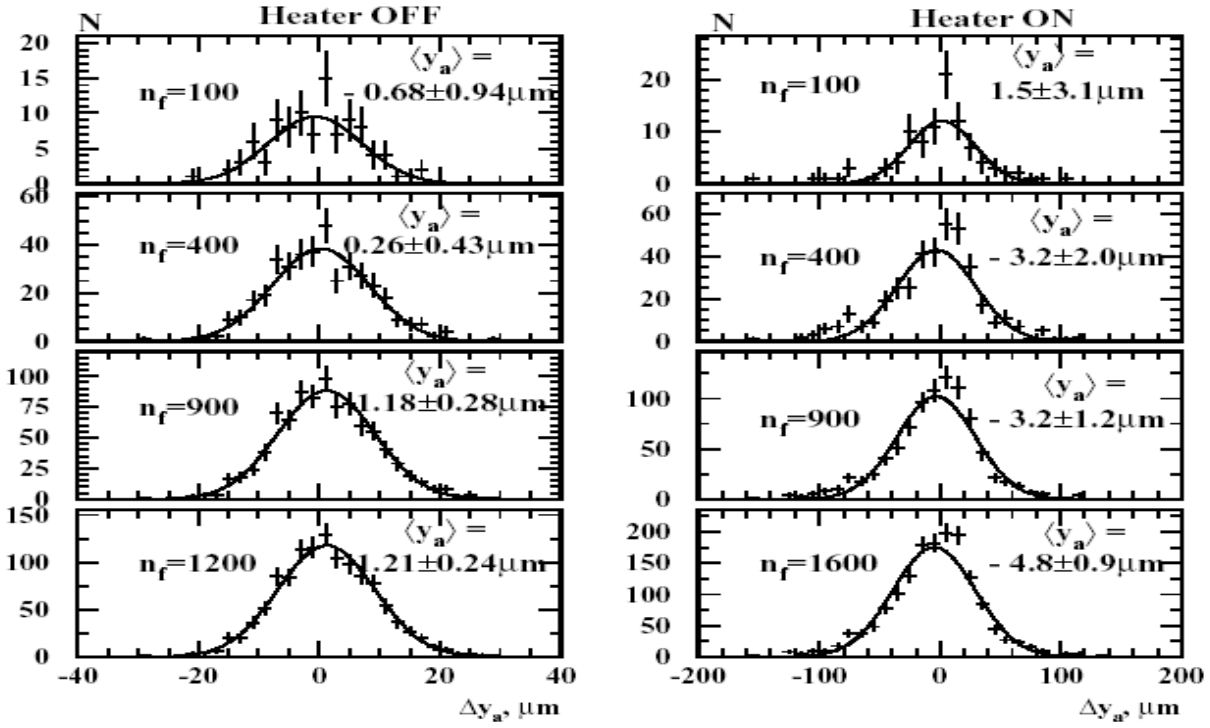

Figure 14 Accuracy of the measurement of the relative movements of the light source and CCD in the homogeneous (left part) and heated (right part) air media as function of the number of readings

These values turn out to be better than what is expected from Eq. (6), which gives $\sigma(\Delta y_a) \approx 12\sigma_m$ ≈ 11 μm at $\sigma_m \approx 0.9$ μm in the homogeneous medium (c.f. Figure 7) and $\sigma(\Delta y_a) \approx 480$ μm at σ_m ≈ 40 μm at the heater switched on (c.f. Figure 8). The explanation of the large "discrepancy" in the inhomogeneous case is as follows. The error given by Eq. (6) is evaluated for independent (uncorrelated) $\Delta y(UV)$ and $\Delta y(IR)$. This is not the case for the heated medium, where the variations of $\Delta y(UV)$ and $\Delta y(IR)$ are caused mainly by thermal turbulence effects which engender strong positive correlations between $\Delta y(UV)$ and $\Delta y(IR)$ (c.f. Figures 3, 6, 10, 11). Since $\Delta y(UV)$ and $\Delta y(IR)$ enter Eq. (4) with opposite signs, their positive correlations reduce the dispersion of the reconstructed displacement Δy_a. In what concerns the accuracy of the reconstruction of the mean value of Δy_a, it is seen from Figure 14 that for large reading numbers ($n_f > 900$) it reaches ≈ 0.25 μm in the homogeneous case and ≈ 1μm in the heated medium.

Figure 15 demonstrates the long–period (8 hours) measurement of the mean values of the displacements Δy_a and Δx_a reconstructed with the help of the data set presented in Figure 11 (let us remind that each point on Figure 11 is obtained by integrating over 1000 readings). The error

for each point is about 1 μm, allowing to monitor the displacements which are as small as a few microns.

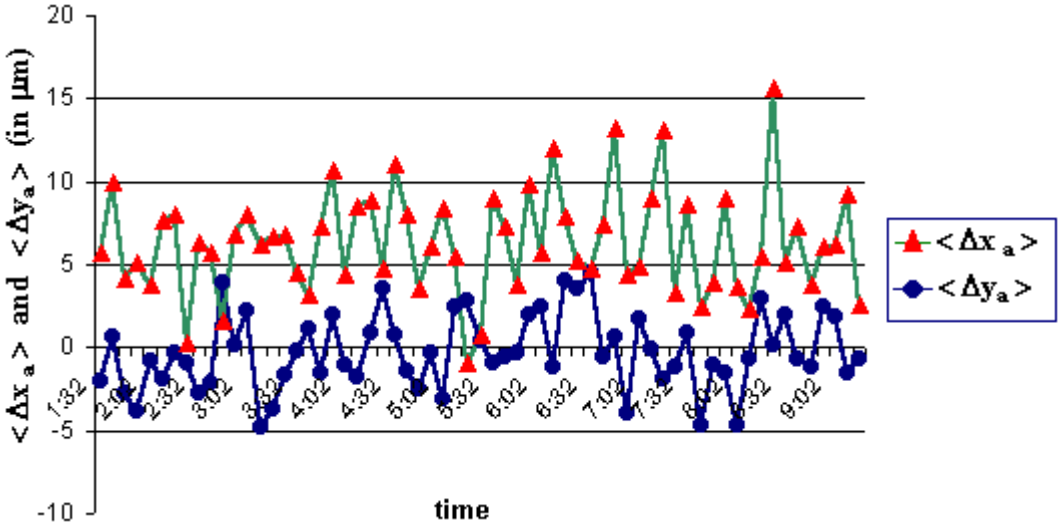

Figure 15 Relative movements of the LED and CCD in horizontal and vertical directions extracted by the two-lambda method (the mean value of the vertical temperature gradient is – 1.7° C/cm).

The quoted values of Δy_a and Δx_a do not include the uncertainty related to that in the used value of r. As it was shown in Section 2, the latter is sensitive to the value of $\lambda(UV)$ but does not practically 'feel' the value of $\lambda(IR)$. The measured emission spectrum of the UV LED results in $<\lambda(UV)>$ = 354 nm with a FWHM value of 10 nm. In view of the spectral dependence of the photosensor sensitivity, the UV light 'seen' by the CCD has an effective wavelength $<\lambda(UV)>_{eff}$ ≈ 360±5 nm, the quoted error being caused by the uncertainties in the photosensor spectral response. As a result, the true value of r turns out to be within r = 1.128±0.005. For boundary values of r, the mean values of the reconstructed displacements averaged over 8 hours are: a) $<\Delta y_a>$ = –2.0±2.3 μm and $<\Delta x_a>$ = 11.0±3.3 μm for r = 1.133 and b) $<\Delta y_a>$ = 1.6±2.3 μm and $<\Delta x_a>$ = 11.9±3.3 μm for r = 1.123. One therefore concludes that $<\Delta x_a>$ is rather insensitive to the choice of r, while the uncertainty in r results in a slightly larger dispersion of $<\Delta y_a>$, $\sigma(\Delta y_a)$ ≈ 3 μm.

5. SUMMARY. FURTHER STEPS.

Our work demonstrates a principal possibility to extend the applicability of the optical monitoring systems to the measurement of the relative displacements of the geometrical objects in thermally inhomogeneous environment. An experimental setup which operates with two LED sources at $\lambda(UV)$ = 360 nm and $\lambda(IR)$ =1000 nm is constructed and tested at different temperature gradients of the air medium. The measured deflections of the UV and IR beams and their ratio are found to be consistent with theoretical expectations. It is demonstrated, that a simultaneous measurement of the deflections of the two exploited beams allows to infer the relative displacements of the light source and photosensor with a precision of a few microns.
An advantage of our approach is that it deals with low-cost LED sources. Furthermore, the UV light, we used, has smaller wavelength (providing hence better measurement accuracy) than the second, UV, harmonics (430 nm) of the dual-wavelength laser emitter presented in [9,10]. In

order to increase the accuracy of our measurements, we have purchased a λ = 254 nm hydrogen light source, which is produced by the US MaxMax Company [15]. This can give a noticeable gain in the measurement accuracy. Unfortunately, the λ_2 = 254 nm light is beyond the spectral response range of the known to us not too expensive CCDs and we are considering a possibility to use other sensors for the detection of this light. A possible candidate could be the four-sector photodiode sensors used in [4] and [9,10].

We are also considering the development of a setup with three (two IR and one UV) or four (two IR and two UV) light beams, which can provide monitoring of 3D movements of the objects, including relative axial displacements and rotations. The distance between two identical (e.g. IR) light spots on CCD does not change either due to relative displacements of the light source and the CCD in *x*– or *y*–directions or due to the thermal gradient. However, this distance changes due to the displacement along *z*–axis and the latter can be inferred from the CCD data (although with a worse accuracy). In what concerns the rotation around the *z*–axis, it can be obtained from the differences of the light spot coordinates $x(IR_1) - x(IR_2)$ and $y(IR_1) - y(IR_2)$ which are sensitive to the rotation around *z*, but do not 'feel' either displacements in *x*– and *y*–directions or thermal gradient.

Further development assumes also the 'compactification' of the setup and construction of a portable version. This will allow exploiting our optical sensor in the "outdoor" experiments, for the monitoring of the movements of the large–scale objects.

6. ACKNOWLEDGEMENTS

We thank Davit Bagdasaryan and Galust Sargsyan for their help at the beginning stage of the setup development. Our work was partially supported by Swiss Fonds Kidagan and Calouste Gulbenkian Foundation.

7. REFERENCES

[1] H. Dekker et al., The RASNIK/CCD 3–Dimensional Alignment System, Proceedings IWAA93, Third International Workshop on Accelerator Alignment, CERN, Geneva, December 1993

[2] K. Hashemi et al., ATLAS notes ATL–MUON–2000–024 and ATL–MUON–2000–026

[3] W. Blum, H. Kroha, P. Widman, Nucl. Instr. Meth., 1995, Vol. 367, p. A413; ibid.,1996, Vol. 377, p. A404

[4] V.D. Danielyan et al., Reflected light monitor for multi–point position measurements, ALICE Internal Note, ALICE–INT–1999–27

[5] J.Y. Grossiord, G. Jacquet, Yu. Margaryan, The RELCAM, an optical transparent sensor for geometry alignment and monitoring system, ALICE Internal Note, ALICE–INT–2002–19

[6] A.A. Grigoryan and A. Teymurazyan, Light ray displacements due to air temperature gradient, ALICE Internal Note, ALICE–INT–2000–13

[7] Gerald Dicker, Linearity, resolution and systematic errors of the CCD–RASNIK Alignment System, http://www.nikhef.nl/pub/departments/et/ccd_rasnik/code/report.pdf

[8] A. M. J. Huiser, B. F. Gächter, A solution to atmospherically induced problems in very high-accuracy alignment and levelling, Applied Physics, 1989, Vol. 22, p. 1630.

[9] H. Ingensand, B. Boeckem, A high-accuracy alignment system based on the dispersion effect, Proceedings IWAA97, Fifth International Workshop on Accelerator Alignment, ANL/FNL, 13–17 October 1997

[10] B. Boeckem, High-accuracy alignment based on atmospherical dispersion – technical approaches and solutions for the dual-wavelength transmitter, Proceedings IWAA99, Sixth International Workshop on Accelerator Alignment, ESRF, Grenoble, 18–22 October 1999

[11] S. Grigoryan, H. Gulkanyan, H. Karayan, Exploiting light beams of different wavelength in the optical monitoring systems, ALICE Internal Note, ALICE–INT–2001–25

[12] V.D. Bolshakov et al., Radio Geodesic and Electro Optical Measurements, Moscow (and Berlin), 1985 (in Russian and German)

[13] B. Edlen, The Dispersions of Standard Air, J. Opt. Soc. Am., 1953, Vol. 43, n. 5, p. 339

[14] H. Azizbekyan et al., An experimental setup for measurement of the deflection of the light beams of different wavelengths in the thermal inhomogeneous medium, YerPhI Preprint–1585(6)–2003, Yerevan

[15] http://www.maxmax.com